Ultrafast nonthermal terahertz electrodynamics and possible quantum energy transfer in the Nb_{3}Sn superconductor

X. Yang, X. Zhao, C. Vaswani, C. Sundahl, B. Song, Y. Yao, D. Cheng, Z. Liu, P. P. Orth, M. Mootz, J. H. Kang, I. E. Perakis, C.-Z. Wang, K.-M. Ho, C. B. Eom, and J. Wang

Phys. Rev. B **99**, 094504 — Published 7 March 2019

DOI: 10.1103/PhysRevB.99.094504

Ultrafast Non-thermal Terahertz Electrodynamics and Possible Quantum Energy Transfer in a Nb_3Sn Superconductor

X. Yang[1], X. Zhao[1], C. Vaswani[1], C. Sundahl[2], B. Song[1], Y. Yao[1], D. Cheng [1], Z. Liu [1], P. P. Orth[1], M. Mootz[3], J. H. Kang[2], I. E. Perakis[3], C-Z Wang[1], K-M Ho[1], C. B. Eom[2] and J. Wang[1]

[1]*Department of Physics and Astronomy and Ames Laboratory, Iowa State University, Ames, Iowa 50011, USA.*

[2]*Department of Materials Science and Engineering, University of Wisconsin-Madison, Madison, WI 53706, USA.*

[3]*Department of Physics, University of Alabama at Birmingham, Birmingham, AL 35294-1170, USA.*

(Dated: February 19, 2019)

We report terahertz (THz) electrodynamics of a moderately clean A15 superconductor (SC) following ultrafast excitation to manipulate quasi–particle (QP) transport. In the Martensitic normal state, we observe an photo-enhancement in the THz conductivity using optical pulses, while the opposite is observed for THz pump. This demonstrates *wavelength-selective* non-thermal control of conductivity distinct from sample heating. The photo-enhancement persists up to an additional critical temperature, above the SC one, from an competing electronic order. In the SC state, the fluence dependence of pair breaking kinetics together with an analytic model provides an implication for a "one photon–to–one Cooper pair" non-resonant energy transfer during the 35-fs laser pulse, i.e., the fitted photon energy $\hbar\omega$ absorption to create QPs set by $2\Delta_{SC}/\hbar\omega$=0.33%. This is more than one order of magnitude smaller than in previously studied BCS SCs, which we attribute to strong electron–phonon coupling and possible influence of phonon condensation.

The competition and interference between SC and other co-existing electronic instabilities appear to be universal in quantum materials. How to exploit the balance of these orders as a control knob to achieve ultrafast manipulation of quasi–particle (QP) properties is an outstanding challenge. Answering these questions has been proven important not only in the more sophisticated quantum materials [1–3] but also in some well-established systems such as A15 superconductors [4–9]. Recently, a strikingly long-lived, gapless QP quantum phase with coherent transport is demonstrated by THz quench of a Nb_3Sn superconducting gap without heating other degrees of freedom [10]. Nb_3Sn, as a paradigmatic A15 compound, exhibits a Martensitic normal state transition above the superconducting one, which has been ascribed to optical phonon condensation ("dimerization" of Nb atoms) [11], possibly driven by a Van Hove singularity (VHS)-like electronic density-of-states peaked at $\sim E_F$ and by strong electron-phonon interaction [5–8, 12, 13]. The order parameters competing with SC likely exhibit multiple components, both lattice and electronic, e.g., the apparent splitting of the three-fold degenerate Γ_{12} band concurrently with an elusive electronic or possibly charge-density-wave(CDW)-like order contribution inferred both from tunneling [9, 13, 14] and Raman spectroscopy [15]. As a result, the partial Fermi surface gapping, $\Delta_W \gg \Delta_{SC}$ associated with the Martensitic anomaly affects the electronic states near E_F differently from the competing SC order Δ_{SC} [7]. This opens an opportunity for exploring ultrafast non-thermal manipulation of conductivity via wavelength-selective pumping.

THz spectroscopy is a powerful tool for *quantitative* studies of SC states both in– and out–of–equilibrium. Arising from energy scales in the vicinity of SC gaps Δ_{SC} of few meV, terahertz (THz) electrodynamics, characterized by the complex optical conductivity response function $\tilde{\sigma} = \sigma_1(\omega) + i\sigma_2(\omega)$, is a direct measure of both dissipation of QPs and inductivity of SC condensate. Prior THz studies of SC samples mostly revealed "conventional" features in the deep impurity limit, $\hbar/\tau_{imp} \gg 2\Delta_{SC}$ [16–18]. In addition, the spectral-temporal dynamics of the order parameters out-of-equilibrium allow the identification of correlation gaps and co-existing orders. These salient features have not been studied in A15 superconductors and the much-needed comparisons with other BCS SCs are absent, e.g., MgB_2 and NbN without competing orders [16–18].

In this Letter, we present THz electrodynamics of Nb_3Sn following ultrafast optical and THz excitation. Our results show that the non-equilibrium THz conductivity after fs optical pump excitation ($\sim$1.55eV) gains an additional spectral weight that, strikingly, persists far above the superconducting T_C, while THz pump ($\sim$4meV) shows a reduced THz conductivity. This *wavelength-selective* control of conductivity is not only distinct from sample heating but also goes beyond the conventional picture of ultrafast melting of competing orders. Furthermore, we observe a rapid, SC pair breaking process consistent with strong electron-phonon coupling. This, together with an analytic model, provides implications for a quantum limit, energy transfer during $\sim$35-fs optical pulses, i.e., one high energy photon breaks only one low energy Cooper pair, with the rest of photon energy exciting phonons rather than creating additional QPs. Such "single quanta", initial transfer of photon energy $\hbar\omega$ to QPs is determined by $2\Delta_{SC}/\hbar\omega$=0.33%, a

value extracted from fitting 100s fs and ps pre-bottleneck dynamics.

I. Samples and Basic Characterizations

A Nb_3Sn film 20nm thick was grown by magnetron sputtering on a 1mm Al_2O_3(R-plane) substrate by co-sputtering of Nb and Sn at high temperatures. The ultrafast THz spectroscopy technique is implemented by using three pulses [10, 19, 20]: optical or THz pump $E_{op/THz}$, THz probe E_{THz} by optical rectification, and optical gating pulse at time t_{gate} for electro-optic sampling. The setup was driven by a 1 kHz Ti:Sapphire regenerative amplifier with 35 fs duration at 800 nm center wavelength.

The equilibrium time-domain THz transmission field and electrodynamics are shown in Figs. 1(a) and 1(b)-1(c), respectively, as a function of temperature. The 4.1 K traces exhibit a diverging $1/\omega$ response in σ_2, arising from reactive SC condensate, and a dissipationless conductivity, witnessed in σ_1 below $2\Delta_{SC}$ =5.1 meV. A finite σ_1 peak at the lowest frequencies <3 meV originates from intraband absorption of the thermally excited Bogoliubons. Such conductivity features of SC diminish when approaching T_c, as seen in the 10-15 K measurements shown in Figs. 1(b)-1(c). As shown in the 16 K and 18 K traces, the normal state exhibits a Drude response: a gapless $\sigma_1(\omega)$ and gradually decreasing $\sigma_2(\omega)$ towards low frequencies. The relatively narrow linewidth of $\sigma_1(\omega)$ indicates a much smaller impurity scattering rate, $\hbar/\tau \sim$7 meV, than in previous THz studies [16–18]. This also leads to more than two orders of magnitude larger l/ξ ratio of mean free path over coherence length in our sample, where $l = v_F\tau$ =32 nm$\sim$4.5-8ξ_{exp} indicative of a moderately clean SC (supplementary).

We now extract the optical self energy $\Sigma(\omega, T)$ using an extended Drude model [21], which provides information complementary to $\widetilde{\sigma}(\omega)$ and more relevant to characterize impurity scattering and correlation. Figs. 1(d) and 1(e) present the complex $\Sigma(\omega, T)$ in terms of the frequency-dependent mass renormalization $m^*(\omega)/m_0$ and momentum scattering rate $1/\tau(\omega)$, which relate to the real and imaginary parts of the $\Sigma(\omega, T)$, respectively. We emphasize three key observations in the SC state. First, the $1/\tau(\omega)$ spectra in Fig. 1(e) clearly reveal a SC gap opening and suppresses the scattering rate below $2\Delta_{SC}$ and reduces it to zero at 4.1K. Second, sharp impurity peaks, commonly seen in dirty limit SC samples at $2\Delta_{SC}$ [21], are absent in $1/\tau(\omega)$ and replaced by a broad cusp in $m^*(\omega)/m_0$ above $2\Delta_{SC}$. Third, $m^*(\omega)/m_0$ in the SC state as $\omega \to 0$ reflects n/n_s, i.e., the ratio between the electron density n and the superfluid density n_s. Here, $n/n_s(4.1K) = m^*(\omega = 0, 4.1K)/m_0 \sim 1.34$ indicates that $\sim$75% of the electrons participate in superfluidity, consistent with the superfluid density ratio ($\sim$70%) obtained from the optical sum rule $\int_{0+}^{\infty}(\sigma_1^n(\omega) - \sigma_1^s(\omega))\, d\omega = \frac{\pi}{2}\frac{n_s e^2}{m}$. This measured n_s/n is $\sim$6 times larger than in superconducting Pb [21].

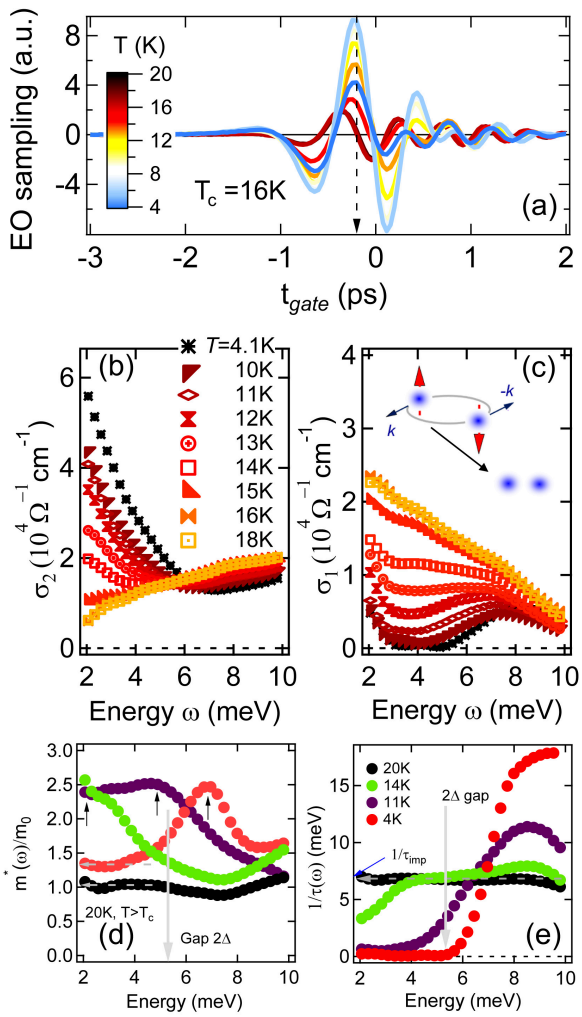

FIG. 1. (Color online). (a) THz probe transmitted field E_{probe} as function of gate delay time t_{gate} for the thermal equilibrium state from 4K to 20K. (b), (c) Temperature dependence of imaginary and real parts of the conductivity, $\sigma_1(\omega)$ and $\sigma_2(\omega)$. Inset to (c): schematic of Cooper pair breaking. (d) Mass renormalization m^*/m and (e) momentum scattering rate $1/\tau$ spectra calculated from $\sigma_2(\omega)$ and $\sigma_1(\omega)$ in (b), (c). Grey solid line denotes $2\Delta_{SC}$ gap at 4.1K. Dashed lines mark the asymptotic m^*/m and $1/\tau$ towards zero frequency.

Next we simulate the static THz conductivity of Nb_3Sn by Mattis-Bardeen (MB) model used for type I, dirty limit superconductors. It has been used extensively in prior studies [16–18] and successfully accounts for the measured THz electrodynamics in both NbN and MgB_2 superconductors. Given the normal state conductivity $\sigma_1(\omega)$ at 16K, MB model reproduces THz response function of Nb_3Sn at various temperatures plotted in Fig. 2, Simulation results present a clear deviation from ex-

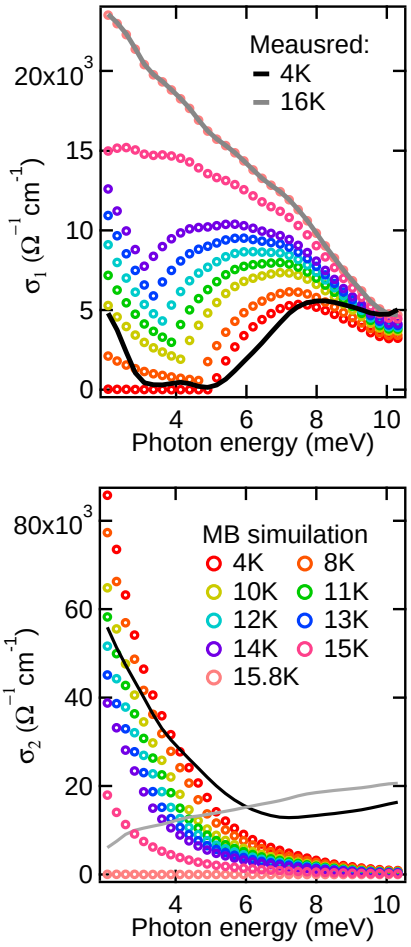

FIG. 2. (Color online). Temperature dependent THz conductivity $\sigma_1(\omega)$ (on top) and $\sigma_2(\omega)$ (on bottom) at 4K, 16K compared to simulation done by Mattis-Bardeen theory

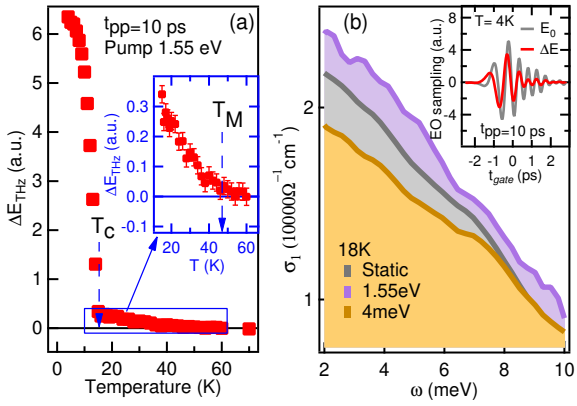

FIG. 3. (Color online). (a) Temperature dependence of pump induced change ΔE_{probe} under $4.02\mu J/cm^2$ excitation fluence. ΔE_{probe} above T_c is magnified in inset to (a), in which Martensitic transition temperature T_M=48K is marked by a blue dashed line. (b) Transient state $\sigma_1(\omega)$ at 10 ps after 1.55eV (purple), 4meV (amber) photo-excitation compared to thermal equilibrium (gray) at 18K. Inset to (b) Transmitted E_{probe} through unpumped Nb_3Sn film (gray) and pump induced change ΔE_{probe} (red).

periment data in Fig.1(b)-(c) (main text). For example, simulated $\sigma_2(\omega)$ is much smaller than measured values at 15.5K, while showing larger divergence at 4K towards zero frequency. This comparison demonstrates that cleanness of superconductor sample is crucial for accounting the measured THz electrodynamics in the vicinity of SC gap, which differentiates THz electrodynamics of cleaner Nb_3Sn from prior THz results on dirty samples.

II. Ultrafast THz Probes of Martensitic Phase

Next we study ultrafast dynamics of the Martensitic normal state in Nb_3Sn. In Fig. 3(a) we record the photoinduced THz field peak-to-peak amplitude as a function of temperature from 4K to 70K. The measured raw THz field data is shown in the time domain in Fig. 3(b) (inset), including the pump induced change, $\Delta E(t)$, at a fixed pump-probe delay $\Delta\tau_{pp}$=10 ps (red) and the transmitted field through the unexcited sample, $E_0(t)$ (gray).

Two transitions are visible in Fig. 3(a). As expected for a SC, the photoinduced signal drops significantly at T_C ~16K. Unlike in a conventional SC, however, the signal persists into the normal state and completely vanishes only at a much higher temperature T_M ~47 K (inset). Intriguingly, the latter transition in the THz field amplitude coincides with the Martensitic anomaly associated with the structural-electronic instabilities [5–8, 11–13]. Inset, Fig. 3(b), reveals such additional order parameter with a critical temperature T_M.

The correlation gap Δ_W associated with the Martensitic order inferred from scanning tunneling spectroscopy is ~80 meV [13] as a CDW-like feature which is out of the spectral window studied here which make the Martensitic order relatively "blind" in the low frequency *equilibrium* conductivity spectra. First, unlike typical density wave orders where a significant spectra weight transfer , from low to high frequency develops in conjunction with establishment of the correlation gap, the Martensitic order represents a very subtle partial gapping of Fermi surface. Our data in Fig. 4 measures this low frequency conductivity in the normal state Nb_3Sn that allows the determination of a very small spectra weight change in the range of 1-10 meV. Second, temperature dependence of static optical conductivity in Nb_3Sn is affected by two competing effects in the normal state: increased scattering rate and suppressed Martensitic gap Δ_W. As shown in Fig. 4, spectral weight and slope of $\sigma_1(\omega)$ decreases simultaneously as temperature increases, i.e., scattering rate increase is more significant than spectral weight transfer above SC critical temperature T_c, which results in a decrease of spectra weight in the 1-10 meV by ther-

mal broadening with increasing lattice temperature. It is worth noting that such a decrease of the spectral weight at elevated temperatures is opposite to the strong density wave materials that show an increase of the spectral weight. Such thermal effect makes it difficult to underpin the *non-thermal* suppression of CDW gap from the measured ultrafast conductivity. On the flip side, the above-mentioned issues show that the pump-probe measurement in Fig. 3 with superior signal-noise ratio represent a powerful method to probe study subtle change of Martensitic phase with a clear transition temperature at 47K. The pump-induced increase of spectral weight indicates a distinct non-thermal ultrafast softening of the correlation gap since laser-induced heating will decrease the spectra weight after the pump. Therefore, this demonstrates the clear ultrafast measurement of the Martensitic order and non-thermal melting of its correlation gap.

Next we also demonstrate *wavelength-selective* non-thermal control of conductivity in Nb_3Sn below. The competing T_M order above SC allows such control by tuning the pump between the optical and THz frequency range above or below the correlation gap Δ_W. We start with the normal state at 18K slightly above T_C. The non-equilibrium $\sigma_1(\omega)$ data is shown in Fig. 3(b) for 1.55eV (optical, purple) and 4meV (THz, yellow) pump photon energy. After 1.55eV pump excitation (black), the low frequency conductivity $\sigma_1(\omega)$ gains an additional spectral weight over its equilibrium (no pump) values (gray shade), which is responsible for the non-vanishing, pump-induced signals ΔE_{THz} in the normal state below T_M shown in Fig. 3(a). This pump-induced enhancement is consistent with non-thermal softening of the correlation gap that develops at the T_M transition from Γ_{12} phonon condensation (dimerization) and/or electronic VHSs, by optical excitation with $\hbar\omega_{op} \gg \Delta_W$. Such softening gives rise to spectral weight transfer to the Fermi surface from high energies above Δ_W. Note that laser-induced heating will only decrease the THz spectral weight after the pump in Nb_3Sn as shown in Fig. 3. The absence of spectral weight increase by thermal broadening in the Martensitic normal state results from very subtle partial gapping of the Fermi surface, opposite to typical CDW materials. Most intriguingly, by changing the pump photon energy to 4 meV, i.e., $\hbar\omega_{THz} \ll \Delta_W$, we observe pump-reduced (purple) instead of pump-enhanced conductivity (brown) shown in Fig. 3(b). This opposite behavior indicates that photoexcitation at sufficiently low frequencies fails to strongly quench the Δ_W gap and, instead, depletes the Fermi sea portion with a non-thermal, threshold behavior [10, 22]. In all cases, the observed pump-wavelength-dependent beavior represents a direct evidence for ultrafast non-thermal control of the THz conductivity by tuning pump photoexcitation above (correlation gap melting) and below (Fermi sea partial depletion) Δ_W. Note that the unusual pump wavelength dependence is absent in previously studied CDW/SDW materials [2, 3, 23] and

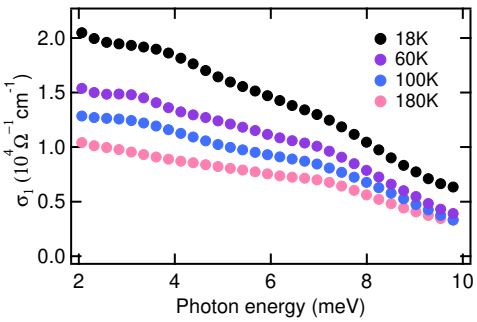

FIG. 4. (color online). Normal state static THz conductivity $\sigma_1(\omega)$ at temperature from 18K to 180K.

BCS SCs without co-existing orders [16–18]. The distinct non-thermal photoexcitation control of QP conductivity provides evidence for an additional electronic instability associated with the Martensitic anomaly beyond the conventional structural one.

III. "One Photon-One Cooper Pair" Quantum Energy Transfer during the Laser Pulse ~30 fs

We turn to the non-equilibrium Cooper pair breaking (CPB) responses in the superconducting state after fs optical excitation. For $\hbar\omega_{op} >> 2\Delta_{SC}$, CPB processes can be driven by multiple interactions between the condensate and photoexcited QPs or high frequency phonons (HFPs). Previous works have shown that majority of the absorbed photon energy subsequently transfers to the phonon reservoir during the fs excitation, which continues to break Cooper pairs [16, 17]. Figs. 5(a) and 5(b) plot the non-equilibrium THz conductivity $\sigma_1(\omega)$ and $\sigma_2(\omega)$ of Nb_3Sn, for various fluences of 1.55eV pump photoexcitation at T=4.1 K. We observe very similar spectral shapes to those seen at various temperatures in equilibrium (Fig. 1). Photo-induced QPs gradually close the SC gap $2\Delta_{SC}$. At the same time, the low frequency $1/\omega$ divergence in σ_2 diminishes with increasing pump fluence I_{pump}. SC features disappear simultaneously above $4\mu J/cm^2$. The thermalized gap $\Delta_{SC}(I_{pump})$ and the superfluid density n_s, readily seen from transient THz spectra quickly diminish as I_{pump} approaches the same fluence. An elevated elecron/lattice transient temperature T^* established after the pump can be extracted by fitting the conductivity data. As shown in the inset of Fig. 5(b), $T^* \rightarrow T_c$ is clearly visible at the quenching fluence $\sim 4\mu J/cm^2$. Therefore, conductivity at Δt_{pp}=10 ps for $T<T_C$ is consistent with previous T^* model of non-equilibrium superconductivity [21, 24, 25].

We track the early time, pair breaking dynamics prior to the establishment of a T^* quasi-equilibrium temperature regime due to scattering of condensate with HFPs and hot QPs. The experimentally–observed ultrafast

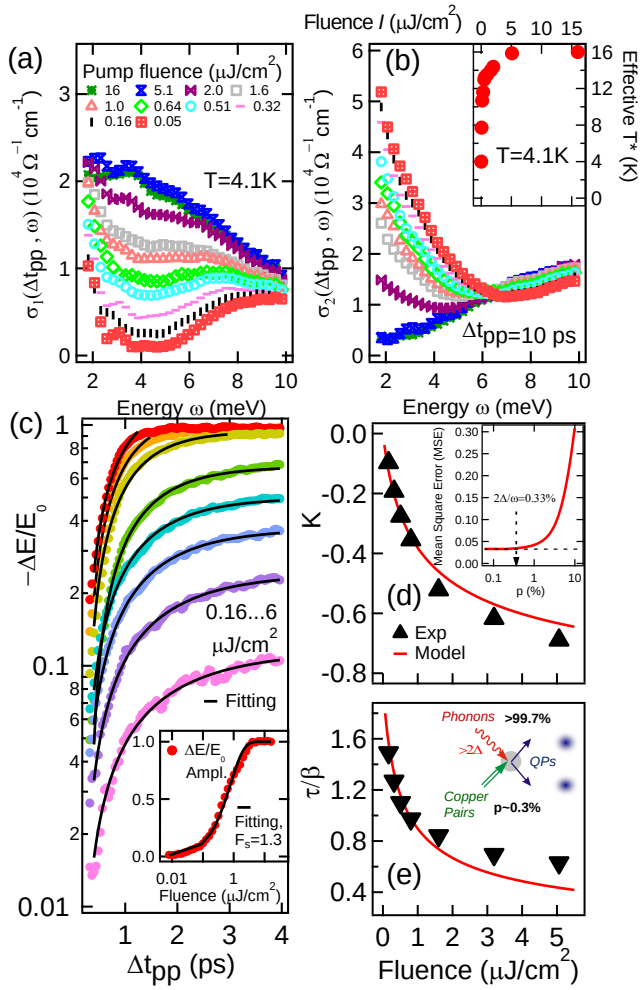

FIG. 5. (color online). (a), (b) Post-pump conductivity $\sigma_1(\omega)$ and $\sigma_2(\omega)$ at t_{pp}=10ps under 0.05–16μJ/cm^2 pumping fluence. Inset to (b) shows effective temperature T* at various fluences. (c) Pump-probe dynamics $\Delta E/E$ measured in experiment (colored dots) are fitted by RT model (black lines). Inset to (c) shows the fitting results of $\Delta E/E$ at $t_{pp} = 10ps$, 4K by saturation curve $(1 - exp(-I/F_s))$, in which I is the pumping fluence and $F_s = 1.3\mu J/cm^2$. (d), (e) Fluence dependent parameters K and τ/β (black triangle) are fitted by Ω and fluence independent {R, β, p} (red line). Inset to (d) Mean square error (MSE) of {R, β} by varying p. Inset to (e) shows the microscopic CPB process.

THz signals for various pump fluences, which reflect the photoexcited QP density n(t), are presented in Fig. 4(c). They show faster CPB with increasing pump fluence during the first 4 ps. In order to reveal the microscopic energy transfer among various reservoirs, we model the CPB kinetics based on the widely used, Rothwarf-Taylor (RT) model [26] that is extensively discussed in [25]. This model is expected to be valid at later ps timescales following the "initial condition" created during the very early 10's fs regime of ultrafast dynamics dominated by electron-phonon coherences and by quasi-particle and phonon nonthermal populations created during the laser pulse. The dynamics after this initial regime is characterized by QP and HFP densities, n(t) and N(t), described by two coupled differential equations [16, 17, 25, 26]. The rise of n(t) in time originates from the pre-bottleneck, CPB process preceding the QP relaxation, which can be described by the analytical expression [25]:

$$n(t) = \frac{\beta}{R}[-\frac{1}{4} - \frac{1}{2\tau} + \frac{1}{\tau}\frac{1}{1 - Kexp(-t\beta/\tau)}], \quad (1)$$

where K and τ are dimensionless parameters determined by the initial conditions: $K = ((\tau/2)/(4Rn_0/\beta+1)-1)/((\tau/2)/(4Rn_0/\beta+1)+1))$and $\frac{1}{\tau} = \sqrt{1/4 + 2R/\beta(n_0 + 2N_0)}$. Here, β is the CPB probability by absorption of HFP and R is the bare QP bi-molecular decay rate. n_0 and N_0 are the initial QP and HFP densities immediately after fs photoexcitation. β and R are fluence independent parameters under weak excitation limit, when n_0 is much smaller than the material–dependent value β/R. Fig. 5(c) presents the best fits, which show a very good agreement with the data. The fitting parameters τ/β and K are extracted as the function of fluence and plotted in Figs. 5(d) and (e) respectively.

Further quantitative information can be obtained by fitting τ/β and K versus the absorbed energy density Ω. Here Ω at I_q=4.02$\mu J/cm^2$ is equal to the SC condensate energy U=4757mJ/mol [23]. The determination of Ω is critical for this purpose which has been described in details in the supplementary. Given the lack of direct information about the very early 10's fs quantum regime during the laser pulse, we treat the initial condition phenomenologically, which can be extracted from the measured dynamics $\geqslant$250fs and a rigorous error analysis. Denoting the portion of the absorbed energy that initially goes into QP excitation as p, we have n_0=pΩ/Δ and N_0=(1-p)$\Omega/2\Delta$ created by fs photoexcitation. The best fit to the extracted τ/β and K data, obtained by minimizing the mean-square error (MSE) of the parameter set $\{p, R, \beta\}$, is achieved for p=0.2$\pm$0.1%, which gives the values of β^{-1} = 1.0 $\pm$ 0.1 ps and R = 105.5 $\pm$ 10 ps^{-1} unit cell^{-1}. We further plot the MSE of the above fitting as function of p in inset, Fig. 4d by only fitting $\{R, \beta\}$ for each fixed p (supplementary). The further fitting details are described in supplementary. Intriguingly, a strong deviation from the minimum error starts at a very small p$\sim$0.33% that coincides with $2\Delta_{SC}/\hbar\omega$, as marked (dashed arrow) in Fig. 5(d). The fitted 0.33% value implies a quantum limit of the energy transfer process during 35-fs photoexcitation of the A15 system, i.e., one high energy photon, $\hbar\omega$=1.55 eV, breaks only one pair, $2\Delta_{SC}$ =5.1 meV, with simultaneous excitation of phonon populations during initial QP cascading (inset,

Fig. 5(e)). Although a direct measurement of 10s of fs transient state is technically challenging to resolve, this conclusion is consistent with much faster CPB dynamics in Nb_3Sn, as shown in Fig. 5(c), for the first 100s fs. Pump-probe signal saturates within 4ps even at lowest fluence, corresponding to 10% of total cooper pairs breaking. In comparison, under the similar pumping condition it takes tens and even hundreds of ps for NbN and MgB_2 to reach the same condition and maximum of pump-probe signals [16, 17]. Applying the same standard fitting and error analysis leads to at least one order of magnitude lower initial energy transfer in Nb_3Sn than any previously measured BCS SCs: 0.33% here vs. MgB_2 (p∼6%) [16] and NbN (p∼9%) [17].

The possible quantum energy transfer process is consistent with strong electron-phonon couplings in A15 SCs. The value of electron-phonon coupling constant λ can be determined from the relation $R = \frac{8\pi v\lambda\Delta_{SC}^2}{\hbar N(0)\omega_D^2}$. Here ω_D is the phonon cutoff frequency, N(0) is the electronic density of states per unit cell at the Fermi level and v is the number of atoms per unit cell. We obtain $\lambda \approx$ 2.0, which agrees very well with previous estimates of $\lambda \approx 1.8\pm0.15$ [27] and is 2 times larger than in the previously studied NbN. In addition, a much higher phonon-pair scattering probability $\beta \sim 1\text{ps}^{-1}$ is seen in Nb_3Sn as compared to MgB_2 (β=1/15 ps^{-1}) [16] and NbN (β=1/6 ps^{-1}) [17]. Here phonon condensation from Martensitic order already is a part of the SC electronic order which can potentially be much more efficiently excited during the pulse that differentiates the A15 from other SCs.

IV. Discussions on Model Analysis and Energy Transfer

The Cooper pair breaking (CPB) dynamics by high energy photons can be quantitatively analyzed using RT model, which has been applied to NbN [17] and MgB_2 [16] superconductors. Prior experimental studies are summarized in Table I as comparison to our work. The fitting procedure is descried below.

To understand the difference in the fitted values of β (i.e. CPB probability by adsorption of HFP) and R (i.e. bare QP recombination rate) in different systems, we further computed β/R in MgB_2, NbN and Nb_3Sn as it has the dimensionality of concentration and can be expressed in terms of material intrinsic properties:

$$\frac{\beta}{R} = \frac{N(0)^2\pi\omega_D^3}{18\nu\Delta} \tag{2}$$

where $N(0)$ is the electronic density of states (DOS) per unit cell, ω_D is the Debye energy, ν is the number of atomes per unit cell, Δ is the superconducting gap.

The calculated results and other key parameters of different materials (NbN, MgB_2 and Nb_3Sn) are summarized in Table II. Fitted β/R shows a decent agreement with calculated values by Eq.(10). We found that β/R in Nb_3Sn is more than 10 times higher than the other two systems, which is attributed to the much larger DOS at the Fermi level. The different fitting parameters for Nb_3Sn can be readily observed in pump-probe traces. After fs photoexcitation, Nb_3Sn reaches the saturation QPs density at much shorter time compared to NbN and MgB_2. Quantitatively, at optical fluence corresponding to 10% pair breaking, Nb_3Sn takes 4ps to reach the peak of QPs density, an order of magnitude faster than NbN (20ps) [17] and MgB_2 (40ps) [16]. Such behavior is consistent with the much larger pair breaking probability β in Nb_3Sn from fitting.

The above fitting results is obtained under the condition $\Omega \sim U_{BCS}$. Varying Ω only changes value of R without affecting the other two fitting parameters $p = 0.2\%$ and $\beta = 1.0$. Assuming that the optical energy absorption is $\Omega \sim 10U_{BCS}$, this will give R∼10.5 and produces unphysical result for $\beta/R \sim 0.095$ contradicting to Eq. 10. Therefore this cannot be the correct scenario for Nb3Sn. On the other hand, β/R shows a very good agreement with Eq.10 for NbN and MgB_2, when 800nm energy absorption matches well with BCS condensation energy. Further discussion about fitting parameters are described in supplementary.

The non-equilibrium Cooper pair breaking responses in the superconducting state after fs optical excitation can be roughly divided into several temporally overlapping stages. First, quantum non-thermal regime during the optical pulse photoexcitation less than tens of fs. This initial temporal regime is not directly resolved experimentally here, but sets up the initial condition for the ps dynamics that is directly observed in the present experiment (Fig. 5). There is no microscopic theory yet to fully account for this initial regime, which in our A15 system involves coherence and non-thermal populations of both electrons and phonons. The optical phonon condensation in the SC ground state below the Martensitic transition temperature is perturbed by the photoexcitation process, leading to photoinduced electron-phonon dynamics. Since femtosecond pulses are shorter than the characteristic time scales of non-thermal SC dynamics, we have chosen a phenomenological approach based on the standard Rothwarf-Taylor model. The portion of absorbed energy p initially goes into QP excitations without lattice excitation while the rest excites phonon populations both during and after pair-breaking. We thus characterize phenomenologically the initial condition that triggers subsequently the incoherent dynamics after the pulse. Second, pre-bottleneck regime accounts for the formation dynamics of the phonon bottleneck. Here the CPB kinetics can be also based on the Rothwarf-Taylor model, which has been extensively and successfully applied in various SC systems and can be derived microscopically within a Markovia quasi-adiabatic

TABLE I. Comparison of Optical Pump-THz Probe Experiment on NbN, MgB_2 and Nb_3Sn Superconductor

	NbN [17]	MgB_2 [16]	Nb_3Sn
Transport Lifetime	$246cm^{-1}$=22fs	37meV=18fs	8.27meV=80fs
Photoexcitation Pulse Duration	50fs	150fs	35fs
Electron-Phonon Coupling λ	1.1	0.7-0.9	2
p	∼9%	∼6%	∼0.33%

TABLE II. Comparison of the key parameters among NbN, MgB_2 and Nb_3Sn Superconductor

	MgB_2 [16]	NbN [17]	Nb_3Sn
T_c	∼39K	∼15K	∼16K
λ	0.7∼0.9	1∼1.2	1.8±0.15
SC gap Δ	$\Delta_1 = 2.2meV$ $\Delta_2 = 7.2meV$ at 4.2K	$\Delta = 3.07meV$	$\Delta = 2.55meV$
N(0) (spin cell eV)$^{-1}$	0.7	0.88	11.4
ω_D	0.064eV (750K)	0.31eV(363K)	0.02eV(230K)
p	6%	9%	∼0.3%
R (ps^{-1} unit cell^{-1})	100±30	160±20	105±10
β (ps^{-1})	1/(15±2)	1/(6±1)	0.99
Rising time	∼40ps	∼20ps	∼4ps
β/R from fitting (unit cell^{-1})	0.00067	0.001	0.0095
β/R from eq.(10) (unit cell^{-1})	0.001	0.0007	0.0089

approximation. Previous works have shown that the majority of the absorbed photon energy subsequently transfers to the phonon reservoir as high frequency phonons and then continues to break Cooper pairs after the photoexcitations, as shown in Table I and II. Third, bottleneck recovery regime takes place at very long, hundreds of ps time scales. The first two regimes are the focus in this paper.

We emphasize three points. First, what we have observed here, based on evidence extracted from the high quality data and exact analysis, is that, although the tens of fs regime is not directly accessed in our and other experiments, it is still possible to determine p from high signal-to-noise-ratio data obtained during the longer, 100's fs pre-bottleneck time regime. In our case, the extracted initial energy transfer is 0.33%, same as $2\Delta/(\hbar\omega)$ determined by SC gap and photoexcitation energy. Thus, one high energy photon $\hbar\omega$ basically breaks one low energy Cooper pair 2Δ during the coherent excitations of optical pulse of 30 fs (the quantum SC quench regime) accompanied by phonon excitation. We refer the observation of one photon-to-one pair, non-resonant energy transfer during the fs optical excitations as quantum energy transfer. Second, p in in Nb_3Sn is two orders of magnitude smaller than in NbN, MgB_2, as shown in Table II, which provides the much needed comparisons between these samples. Third, our data indicates that phonon emission is much more efficient during the QP de-coherence and population build-up immediately after and during the pulse ∼30 fs. This is consistent with enhanced e-phonon coupling in Nb_3Sn and the optical phonon condensation in the ground state below the Martensitic transition that differentiates A15 from other simpler SCs. Note, however, that the exact microscopic dynamics of quantum quench of superconductivity and build-up of QP population immediately after fs pulse is still lacking which warrant further study for the development of the non-equilibrium quantum quench dynamics of a strongly coupled e-lattice system with optical phonon condensation in the ground state.

V. Conclusion

In summary, We demonstrate ultrafast non-thermal control of the THz conductivity in the Martensitic normal state by tuning the pump photon energy and identify a competing electronic order in the normal state below the Martensitic anomaly in Nb_3Sn. In the SC state, we reveal a possible quantum energy transfer during the initial quantum nonthermal regime which we attribute to strong electron–phonon coupling and optical phonon condensation in the ground state. The distinct ultrafast THz electrodynamics of the model A15 compound with electron-phonon complex order offer perspectives to probe the very early, *fs* pair breaking dynamics in unconventional superconductors [28] and manipulate other competing order systems such as magnetic materials [29–31]

Work at Iowa State University was supported by the Army Research office under award W911NF-15-1-0135 (THz spectroscopy). The theory work was supported by the Ames Laboratory, the US Department of Energy, Office of Science, Basic Energy Sciences, Materials Science and Engineering Division under contract #DE-AC02-07CH11358 (theoretical modeling and numerical

simulations). THz Instrument was supported in part by the Keck Foundation (J.W.). Work at Wisconsin (sample growth and basic characterizations) was supported by the DOE Office of Basic Energy Sciences under award number DE-FG02-06ER46327. The extra analysis done at the University of Alabama, Birmingham was supported by the US Department of Energy under contract#DE-SC0019137 (M.M and I.E.P).

[1] T. Li, A. Patz, L. Mouchliadis, J. Yan, T. A. Lograsso, I. E. Perakis and J. Wang Nature **496**, 69 (2013).
[2] A. Patz, T. Li, S. Ran, R. M. Fernandes, J. Schmalian, S. L. Budko, P. C. Canfield, I. E. Perakis and J. Wang, *et al. Nat. Commun.* **5**, 3229 (2014).
[3] M. Porer, U. Leierseder, J. M. Mnard, H. Dachraoui, L. Mouchliadis, I. E. Perakis, U. Heinzmann, J. Demsar, K. Rossnagel, and R. Huber, Nature Materials **13**, 857 (2014).
[4] M. Kataoka, Journal of Physics C: Solid State Physics, **19**, 2939-2962 (1986).
[5] R. N. Bhatt, Phys. Rev. B **16**, 5, (1977).
[6] W. Weber and L. F. Mattheiss, Phys. Rev. B **25**, (1982).
[7] G. Bilbro and W. L. McMillan, Phys. Rev. B **14**, 1887-1892 (1976).
[8] B. Sadigh and V. Ozolinš, Phys. Rev. B **57**, 2793 (1998).
[9] J. K. Freericks, A. Y. Liu, A. Quandt, and J. Geerk, Phys. Rev. B **65**, 224510 (2002).
[10] X. Yang, C. Vaswani, C. Sundahl, M. Mootz, P. Gagel, L. Luo, J. H. Kang, P. P. Orth, I. E. Perakis, C. B. Eom and J. Wang, Nature Materials, **17**, 586 (2018).
[11] G. Shirane, and J. D. Axe, *Phys. Rev. B* **4**, 2957 (1971).
[12] R. S. Markiewicz, J Phys. Chem. Solids, **58**, 1179 (1997)
[13] R. Escudero, F. Morale, Solid State Commun. **150**, 715-719 (2010).
[14] See. e.g., T. Ekino, A. M. Gabovich, A. Sugimoto, Y. Sakai and J. Akimitsu, Superconductors–New Developments (DOI: 10.5772/58655), Chapter **4**, 55-72 (2015).
[15] For review, see, e.g., T. P. Devereaux and R. Hackl, Rev. Mod. Phys. **79**, 175 (pg. 202-205) (2007)
[16] J. Demsar, R.D. Averitt, A. J. Taylor, V. V. Kabanov, W. N. Kang, H. J. Kim, E.M. Choi and S.I. Lee, *Phys. Rev. Lett.* **91**, 267002 (2003).
[17] M. Beck, M. Klammer, S. Lang, P. Leiderer, V. V. Kabanov, G. N. Goltsman, and J. Demsar, Phys. Rev. Lett. **107**, 177007 (2011).
[18] R. Matsunaga and R. Shimano, Phys. Rev. Lett. **109**, 3 (2012).
[19] L. Luo, I. Chatzakis, A. Patz, J. Wang, Phys. Rev. Lett. **114**, 107402 (2015).
[20] L. Luo, X. Yang, X. Liu, Z. Liu, C. Vaswani, D. Cheng, M. Mootz, X. Zhao, Y. Yao, C.Z. Wang, and K.M. Ho, J. Wang, Nature Communications, doi.org/10.1038/s41467-019-08559-6 (2019).
[21] T. Mori, E. J. Nicol, S. Shiizuka, K. Kuniyasu, T. Nojima, N. Toyota, and J. P. Carbotte, Phys. Rev. B **77** (2008).
[22] X. Yang, et al., in preparation (2010)
[23] J. S. Kim, G. N. Tam, and G. R. Stewart, Phys. Rev. B **92**, 224509 (2015).
[24] C. S. Owen and D. J. Scalapino. *Phys. Rev. Lett.*, **28**, 1559 (1972).
[25] V. V. Kabanov, J. Demsar, and D. Mihailovic, Phys. Rev. Lett. **95**, 147002 (2005).
[26] A. Rothwarf and B. N. Taylor, Phys. Rev. Lett. **19**, 27 (1967).
[27] E.L. Wolf, J. Zasadzinski, G.B. Arnold, D.F. Moore, J.M. Rowell and M. Beasley, Phys. Rev. B **22**, 1214 (1980).
[28] X. Yang, L. Luo, M. Mootz, A. Patz, S.L. Budko, P.C. Canfield, I.E. Perakis, and J. Wang *Phys. Rev. Lett.* **121**, 267001 (2018)
[29] A. Patz, T. Li, L. Luo, X. Yang, S. Bud'ko, P.C. Canfield, I.E. Perakis and J. Wang, *Phys. Rev. B* **95**, 165122 (2017); A. Patz, T. Li, X. Liu, J.K. Furdyna, I.E. Perakis, and J. Wang *Phys. Rev. B* **91**, 155108 (2015)
[30] P.C. Lingos, A. Patz, T. Li, G.D. Barmparis, A. Keliri, M.D. Kapetanakis, L. Li, J. Yan, J. Wang and I.E. Perakis, *Phys. Rev. B* **95**, 224432 (2017)
[31] J. Wang, G.A. Khodaparast, J. Kono, T. Slupinski, A. Oiwa and H. Munekata, *Physica* **20E**, 412 (2004)
[32] D. C. Mattis, , and J. Bardeen. Physical Review **111.2** (1958): 412.
[33] J. Demsar, R. Averitt , A. Taylor , W. Kang, H. Kim, E. Choi, S. Lee. International Journal of Modern Physics B. 2003 Aug 10; 17(18n20):3675-81.
[34] M. Perpeet, M. Hein, G. Mller, H. Piel, J. Pouryamout, W. Diete. Journal of applied physics. 1997 Nov 15;82(10):5021-3.
[35] T. Orlando, E. McNiff Jr, S. Foner, M. Beasley. Physical Review B. 1979 May 1;19(9):4545.
[36] R. Kaindl, M. Carnahan, J. Orenstein, D.Chemla , H. Christen, H. Zhai, H. Paranthaman, D. Lowndes. Physical review letters. 2001 Dec 28;88(2):027003.
[37] S. A. Kuzmichev, T. E. Kuzmicheva, S. N. Tchesnokov, JETP Letters 99, 295 (2014); I. Mazin, V. P. Antropov, Physica C **385**, 49 (2003).
[38] W. Weber, Phys. Rev. B 8, 5082 (1973); U. Haufe, G. Kerker, and K. H. Bennemann, Solid State Commun. **17**, 321 (1975).
[39] J. Kortus, I. I. Mazin, K. D. Belashchenko, V. P. Antropov, and L. L. Boyer, Phys. Rev. Lett. **86**, 4656 (2001); B. Z. Xu and S. P. Beckman, 2D Mater. **3**, 031003 (2016).
[40] R. Zhang, P. Gao, X. Wang, and Y. Zhou, AIP Adavnces, **5**, 107233 (2015).
[41] S. L. Budko, G. Lapertot, C. Petrovic, C. E. Cunningham, N. Anderson, and P. C. Canfield, Phys. Rev. Lett. **86**, 1877 (2001).
[42] X. J. Chen, V. V. Struzhkin, S. Kung, H. K. Mao, and R. J. Hemley, Phys. Rev. B **70**, 014501 (2004).
[43] L. J. Vieland and A. W. Wicklund, Phys. Rev. **166**, 424 (1968); A. Junod, T. Jarlborg, and J. Muller, Phys. Rev. B 27, 1568 (1983).